Aust. J. Phys., 1976, **29**, 289–304

Extended Theory of Magnon Sideband Shapes. II* Impure Three-dimensional Antiferromagnets

D. D. Richardson

Department of Theoretical Physics, Research School of Physical Sciences, Australian National University; present address: Department of Physics, Cavendish Laboratory, Madingley Road, Cambridge CB3 OHE, U.K.

Abstract

A phenomenological model is given for calculating magnon sideband lineshapes in the absorption spectra of antiferromagnetic crystals. The method allows an exact expression for the lineshape to be obtained when dispersion within the Brillouin zone of both the exciton energy and the exciton–magnon interaction strength is included. The effect of a substitutional spin impurity is calculated exactly, and a simple example is given which approximates the effects of an impurity on a magnon sideband in the antiferromagnetic perovskite $RbMnF_3$. It is thought that the ability of the model to predict the existence of local modes and resonances justifies the simple form of the model Hamiltonians chosen. The pure crystal sideband lineshape can also be well determined from information on the exciton dispersion and the behaviour of the exciton–magnon interaction strength within the Brillouin zone.

1. Introduction

The model presented in this paper is an extension of the ferromagnetic model given in Part I (Richardson 1974; 1976*a*, present issue pp. 273–88). There have been several theories put forward to describe the lineshape of a magnon sideband in an antiferromagnet (Moriya 1966, 1968; Sell *et al.* 1967; Tanabe and Gondiara 1967; Freeman and Hopfield 1968; Loudon 1968; McClure 1968; Moriya and Inoue 1968; Parkinson and Loudon 1968; Tanabe *et al.* 1968; Meltzer *et al.* 1969; Dietz *et al.* 1970; Misetich *et al.* 1971; Petrov and Gaididei 1971; Stokowski *et al.* 1971; Bhandari and Falicov 1972; Eremenko *et al.* 1974; Gaididei and Loktev 1974). Some of these theories are very complex. Following my earlier work, I give here a model which is simple yet still describes the essential features of the physical system and also allows for the description of the effect of a substitutional spin impurity on the sideband. The latter effect has been treated by Parkinson (1969*a*, 1969*b*) who discussed in particular the possible appearance of local modes outside the sideband due to Ni^{2+} impurities in $RbMnF_3$. The work of Parkinson is an extension of the magnon sideband calculation of Parkinson and Loudon (1968). This model is quite complicated and involves several assumptions to obtain a result, and it is difficult to understand the physical implications of the assumptions. The model also does not permit any concrete assessment of the possibility of resonance modes appearing within the sideband.

As illustrated in Part I, the present model may be solved exactly within the limitations of the Hamiltonians chosen, and therefore allows for direct physical understand-

* Part I, *Aust. J. Phys.*, 1976, **29**, 273–88.

ing of the results. The phenomenological Hamiltonians are simple but are found to give an adequate description of the physical features observed and expected to be found in the crystals of interest. It is necessary to consider such simplified forms because of the complexity of the theory introduced by both the intrinsic exciton–magnon interaction and the magnon impurity. It can be shown that the Hamiltonians used here may be obtained from more rigorous forms by means of a time-averaging approximation, as is usually used to handle the Green's functions which arise from the more complicated Hamiltonians (Richardson 1976*b*). It is therefore felt that the present model is justifiable on the grounds of similarity to previous models. Also, because of the exact nature of the calculation and the form of impurity Hamiltonian chosen, it is possible to extend the earlier work to include impurity effects.

The present paper adapts the ferromagnetic model calculation to the calculation for an antiferromagnet, and shows that the previously imposed limitations of wavenumber-independent exciton energy and exciton–magnon interaction strength are not necessary to obtain an expression for the magnon sideband lineshape. To illustrate the effects of an impurity, these conditions are re-imposed and a calculation is given of the effect of a substitutional spin impurity with various impurity parameters on the simple cubic antiferromagnet (perovskite) $RbMnF_3$.

The paper is set out as follows: in Section 2 the Hamiltonians to be used in the model are discussed and the main assumptions made to simplify them are pointed out. In Section 3 the calculation of magnon sideband lineshape in the optical absorption spectrum is given while in Section 4 the phenomenological sideband in $RbMnF_3$ is given, assuming the exciton energy and exciton–magnon interaction strength to be constant throughout the Brillouin zone. Section 5 presents a discussion of the effects of a substitutional spin impurity on the sideband calculated in Section 4. The paper concludes with a discussion of the comparison of the present results with those of the ferromagnet (Richardson 1976*a*) and gives some possible effects of taking a $\boldsymbol{k}$-dependent form for the exciton–magnon interaction strength.

2. Hamiltonians of Antiferromagnetic System

The pure crystal Hamiltonian must have magnon, exciton and exciton–magnon components. In general all three energy contributions will be dispersed within the Brillouin zone. We therefore take the two-sublattice crystal Hamiltonian as

$$\mathscr{H} = \sum_{k} \varepsilon_1(\boldsymbol{k})[\alpha_k^+ \alpha_k + \beta_k^+ \beta_k] + \sum_{k} \varepsilon_2(\boldsymbol{k})[A_k^+ A_k + B_k^+ B_k] + \sum_{k} g(\boldsymbol{k})[\alpha_k^+ A_k + A_k^+ \alpha_k + \beta_k^+ B_k + B_k^+ \beta_k], \tag{1}$$

where the sums over $\boldsymbol{k}$ are over the first Brillouin zone whose unit cell has one atom from each sublattice. In equation (1) α_k, β_k are magnon annihilation operators on sublattices A, B, and A_k, B_k are the corresponding exciton operators. The magnon energy is $\varepsilon_1(\boldsymbol{k})$, the exciton energy is $\varepsilon_2(\boldsymbol{k})$ and the exciton–magnon interaction strength is $g(\boldsymbol{k})$. It is assumed that the two sublattices are completely degenerate, with no exchange of excitations between them.

The magnon dispersion is given by

$$\varepsilon_1(\boldsymbol{k}) = 2JSz(1-\gamma_k^2)^{\frac{1}{2}}, \qquad \text{with} \qquad \gamma_k = z^{-1} \sum_{[\Delta]} \exp(\mathrm{i}\boldsymbol{k}.\Delta), \tag{2a, b}$$

for the nearest neighbour lattice vectors Δ, while J and S are the exchange integral and spin for the pure crystal, and z is the number of nearest neighbours of a magnetic site.

The wavenumber dependences of ε_2 and g are functions of the particular crystal to be studied and of the symmetry at the atom sites. We shall not consider any particular forms for these, though Knox (1963), Loudon (1968) and Callaway (1974) gave good reviews of the Frenkel exciton theory, and Parkinson and Loudon (1968) and Petrov (1971) have discussed the exciton–magnon interaction in some detail. We consider the $\boldsymbol{k}$ dependence of g in Section 6 insofar as it affects the present treatment.

The effects of a substitutional spin impurity on sublattice A are described by the spin Hamiltonian (subscripted I for impurity)

$$\mathscr{H}_{\mathrm{I}} = [\alpha^{+} \quad \beta] \begin{bmatrix} \hat{\mathbf{M}}_1 & \hat{\mathbf{M}}_2 \\ \hat{\mathbf{M}}_3 & \hat{\mathbf{M}}_4 \end{bmatrix} \begin{bmatrix} \alpha \\ \beta^{+} \end{bmatrix}, \tag{3}$$

where

$$\alpha^{+} = [\alpha_{k_1}^{+}; \ldots; \alpha_{k_N}^{+}], \qquad \text{etc.} \tag{4}$$

The submatrices are given by

$$(M_1)_{ij} = 2JSz[\{l_1(\boldsymbol{k}_i)\, l_2(\boldsymbol{k}_j)\, \gamma_{k_j} + l_2(\boldsymbol{k}_i)\, l_1(\boldsymbol{k}_j)\, \gamma_{k_i}\}\gamma + \varepsilon\, l_1(\boldsymbol{k}_i)\, l_1(\boldsymbol{k}_j) + \rho\gamma_{k_i - k_j}\, l_2(\boldsymbol{k}_i)\, l_2(\boldsymbol{k}_j)] + JS^2\rho z\, \delta(i,j), \tag{5}$$

$$(M_2)_{ij} = 2JSz[\{l_1(\boldsymbol{k}_i)\, l_1(\boldsymbol{k}_j)\, \gamma_{k_j} + l_2(\boldsymbol{k}_i)\, l_2(\boldsymbol{k}_j)\, \gamma_{k_i}\}\gamma + \varepsilon\, l_2(\boldsymbol{k}_i)\, l_1(\boldsymbol{k}_j) + \rho\gamma_{k_i - k_j}\, l_1(\boldsymbol{k}_i)\, l_2(\boldsymbol{k}_j)] \tag{6}$$

for

$$\varepsilon = (J'-J)/J, \qquad \gamma = J'J^{-1}(S'S^{-1})^{\frac{1}{2}} - 1 \qquad \text{and} \qquad \rho = (J'S'-JS)/JS, \tag{7a, b, c}$$

where J' and S' are the impurity exchange integral and spin. Submatrices $\hat{\mathbf{M}}_3$ and $\hat{\mathbf{M}}_4$ are given by equations (6) and (5) respectively with l_1 everywhere replaced by l_2 and vice versa. These latter are used to diagonalize the pure crystal magnon Hamiltonian and are

$$l_1(\boldsymbol{k}) = \left(\frac{1-(1-\gamma_k^2)^{\frac{1}{2}}}{2(1-\gamma_k^2)^{\frac{1}{2}}}\right)^{\frac{1}{2}} \qquad \text{and} \qquad l_2(\boldsymbol{k}) = -\left(\frac{1+(1-\gamma_k^2)^{\frac{1}{2}}}{2(1-\gamma_k^2)^{\frac{1}{2}}}\right)^{\frac{1}{2}}. \tag{8a, b}$$

In the present model we assume that points close to the edge of the Brillouin zone contribute most to the regions where the magnon density of states is large. These points correspond to small values of γ_k, so that $l_1^2(\boldsymbol{k}) \to 0$ and $l_2^2(\boldsymbol{k}) \to 1$. If we also consider that the impurity may lie on either sublattice, so that to first order we may replace $\hat{\mathbf{M}}_1$ and $\hat{\mathbf{M}}_4$ by their average, and similarly $\hat{\mathbf{M}}_2$ and $\hat{\mathbf{M}}_3$ by their average, then we have

$$(\overline{M}_1)_{ij} = (\overline{M}_4)_{ij} = \gamma_{ij} \approx 2JSz\varepsilon \equiv \gamma, \tag{9}$$

$$(\overline{M}_2)_{ij} = (\overline{M}_3)_{ij} \approx 0. \tag{10}$$

We therefore ignore the off-diagonal submatrices in equation (3) and consider the diagonal submatrices as identical, with elements independent of wavenumber, i.e. we assume that no excitations are scattered between sublattices by the impurity, so that the latter does not remove the two-sublattice degeneracy of the system. The magnon part of the total crystal Hamiltonian becomes

$$\mathscr{H}_{M+1} = [\alpha^+ \quad \beta^+] \begin{bmatrix} \hat{\mathbf{M}} & \mathbf{0} \\ \mathbf{0} & \hat{\mathbf{M}} \end{bmatrix} \begin{bmatrix} \alpha \\ \beta \end{bmatrix}, \tag{11}$$

where

$$(M)_{ij} = \gamma + \{JS^2 \rho z + \varepsilon_1(\boldsymbol{k}_i)\}\, \delta(\boldsymbol{k}_i, \boldsymbol{k}_j). \tag{12}$$

The magnon sideband will appear in the optical absorption spectrum as a result of the collective interaction of excitons and magnons with photons. We now consider the Hamiltonian for this interaction, which will be used as a perturbation on the crystal (Richardson 1976*b*). It is assumed here that the parent exciton of the sideband is magnetic dipole in character and the sideband itself is electric dipole. Thus, if we neglect the effect of the magnetic component of the applied field, we expect only the sideband to appear in the calculated absorption spectrum.

The form of the perturbation Hamiltonian has been discussed widely in the literature, with good descriptions being given by Loudon (1968), Petrov (1971) and Petrov and Gaididei (1971). The most general form for the crystal field Hamiltonian is

$$\mathscr{H}_X = \boldsymbol{E}\boldsymbol{P}_E \exp(-i\omega t) + HC, \tag{13}$$

where HC is the hermitian conjugate of the first term, and the effective value of $\boldsymbol{P}$ is given by

$$\boldsymbol{P}_E = \sqrt{2} \sum_{k,\mu} \boldsymbol{\Pi}(\boldsymbol{k})(-)^{\mu+1} l_\mu B_\mu^+(\boldsymbol{k}, f)\, b_\mu^+(-\boldsymbol{k}). \tag{14}$$

Here, the sum over μ is over the two sublattices, with the l_μ given by equations (8a) and (8b), while $B(\boldsymbol{k}, f)$ is an exciton annihilation operator for the fth excited state and $b(\boldsymbol{k})$ is a magnon annihilation operator. We may determine $\boldsymbol{\Pi}(\boldsymbol{k})$ from the symmetry of the ion site. It is related to the dipolar moment of the transition of the pair of magnetic ions from opposite sublattices which is induced by the applied electric field $\boldsymbol{E}$ of frequency ω (Eremenko *et al.* 1974). Values of $\boldsymbol{\Pi}(\boldsymbol{k})$ have been given for several crystals (Tanabe *et al.* 1965; Gondiara and Tanabe 1966; Loudon 1968; Parkinson and Loudon 1968; Meltzer *et al.* 1969).

In the present model, we assume $\boldsymbol{\Pi}$ to be independent of wavenumber (though this is not essential) and consider only one excited orbital state. Since the form of equation (14) is the same whether one chooses the indirect exchange mechanism of Tanabe *et al.* (1965) or the direct dipole–quadrupole coupling of Halley and Silvera (1965) for the exciton–magnon part of the perturbation, we need not concern ourselves in the present phenomenological model with the details of the exact nature of the interaction of the crystal with the radiation.

We choose the perturbation Hamiltonian as

$$\mathscr{H}_P = l \sum_k (\alpha_k^+ A_k^+ + \alpha_k A_k + \beta_k^+ B_k^+ + \beta_k B_k), \tag{15}$$

with the symbols having the same meaning as in equation (1). The interaction energy

l is taken to be independent of wavenumber but time-dependent, including the time dependence of the applied electric field. We have assumed that the perturbation will not transfer excitations between sublattices, so the field will not remove the two-sublattice degeneracy.

3. Theory of Magnon Sideband Lineshape

In previous papers, Richardson (1974, 1976*a*) was able to diagonalize the impure crystal Hamiltonian by a two-stage process because the submatrices of the matrix representation of the Hamiltonian were shown to commute with each other. When we assume a $\boldsymbol{k}$-dependence of the exciton energy ε_2 and the exciton–magnon interaction strength g, the submatrices no longer commute and the diagonalization must be done completely in one step.

The Hamiltonian to be diagonalized is that of the impure antiferromagnet discussed in the previous section:

$$\begin{aligned}\mathscr{H} &= \sum_{\boldsymbol{k}} \varepsilon_1(\boldsymbol{k})[\alpha_{\boldsymbol{k}}^+ \alpha_{\boldsymbol{k}} + \beta_{\boldsymbol{k}}^+ \beta_{\boldsymbol{k}}] + \sum_{\boldsymbol{k}} \varepsilon_2(\boldsymbol{k})[A_{\boldsymbol{k}}^+ A_{\boldsymbol{k}} + B_{\boldsymbol{k}}^+ B_{\boldsymbol{k}}] \\ &\quad + \sum_{\boldsymbol{k}} g(\boldsymbol{k})[\alpha_{\boldsymbol{k}}^+ A_{\boldsymbol{k}} + \alpha_{\boldsymbol{k}} A_{\boldsymbol{k}}^+ + \beta_{\boldsymbol{k}}^+ B_{\boldsymbol{k}} + \beta_{\boldsymbol{k}} B_{\boldsymbol{k}}^+] \\ &\quad + \gamma \sum_{\boldsymbol{k},\boldsymbol{k}'} [\alpha_{\boldsymbol{k}}^+ \alpha_{\boldsymbol{k}'} + \beta_{\boldsymbol{k}}^+ \beta_{\boldsymbol{k}'}]. \end{aligned} \tag{16}$$

The secular equation for the eigenvalues of equation (16) may be obtained from row operations on the matrix representation of $\mathscr{H}$. The result is

$$\begin{aligned} D(\lambda) &= \prod_{\boldsymbol{k}} \{\varepsilon_1(\boldsymbol{k}) - \lambda\}^2 \prod_{\boldsymbol{k}'} \{\varepsilon_2(\boldsymbol{k}') - \lambda\}^2 \prod_{\boldsymbol{k}''} \left(1 - \frac{g^2(\boldsymbol{k}'')}{\{\varepsilon_1(\boldsymbol{k}'') - \lambda\}\{\varepsilon_2(\boldsymbol{k}'') - \lambda\}}\right)^2 \\ &\quad \times \left(1 + \gamma \sum_{\boldsymbol{k}'''} \frac{1}{\varepsilon_1(\boldsymbol{k}''') - \lambda - g^2(\boldsymbol{k}''')/\{\varepsilon_2(\boldsymbol{k}''') - \lambda\}}\right)^2. \end{aligned} \tag{17}$$

When $\gamma = 0$, the first three terms of this product lead to the pure crystal density of states. If we write

$$\begin{aligned} D_0(\lambda) &= \prod_{\boldsymbol{k}} [\{\varepsilon_1(\boldsymbol{k}) - \lambda\}\{\varepsilon_2(\boldsymbol{k}) - \lambda\} - g^2(\boldsymbol{k})]^2 \\ &= \prod_{\boldsymbol{k}} [(\lambda - \lambda_0^+)(\lambda - \lambda_0^-)]^2, \end{aligned} \tag{18}$$

where

$$\lambda_0^{\pm}(\boldsymbol{k}) = \tfrac{1}{2}\{\varepsilon_2(\boldsymbol{k}) + \varepsilon_1(\boldsymbol{k})\} \pm [\tfrac{1}{4}\{\varepsilon_2(\boldsymbol{k}) - \varepsilon_1(\boldsymbol{k})\}^2 + g^2(\boldsymbol{k})]^{\frac{1}{2}}, \tag{19}$$

then it will be seen that there are two branches in the pure crystal spectrum: one for values of λ equal to λ_0^+ and the other for λ equal to λ_0^-. The expression (19) is identical in form to the ferromagnetic crystal result in the absence of an impurity (Richardson 1976*b*). Note, however, that each eigenvalue is doubly degenerate (from equation 18) as a result of the two-sublattice degeneracy.

The effect of the impurity on the crystal density of states will be given from the determinant

$$\mathscr{D}(\lambda) = 1 + \gamma \sum_{\boldsymbol{k}} \left[\varepsilon_1(\boldsymbol{k}) - \lambda - \frac{g^2(\boldsymbol{k})}{\{\varepsilon_2(\boldsymbol{k}) - \lambda\}}\right]^{-1}. \tag{20}$$

Richardson (1976*a*) combined the expression for the eigenvalues of the magnon part of the crystal Hamiltonian with that for the eigenvalues of the total Hamiltonian to obtain an expression similar to equation (20) but with λ replaced by $\lambda^{\pm}$, which is a function of the eigenvalues of the magnon part of the Hamiltonian. For simplicity in the present work we define a parameter Λ which, in the limit of ε_2 and g being $\boldsymbol{k}$-independent, becomes the magnon eigenvalue; i.e. from equation (20) we define

$$\Lambda = \lambda + g^2(\boldsymbol{k})/\{\varepsilon_2(\boldsymbol{k}) - \lambda\}. \tag{21}$$

Conversely we have

$$\lambda = \tfrac{1}{2}\{\varepsilon_2(\boldsymbol{k}) + \Lambda\} \pm g(\boldsymbol{k})\, Y_k(\Lambda), \tag{22}$$

where

$$X_k(\Lambda) = \{\varepsilon_2(\boldsymbol{k}) - \Lambda\}/2g(\boldsymbol{k}) \qquad \text{and} \qquad Y_k(\Lambda) = \{X_k^2(\Lambda) + 1\}^{\frac{1}{2}}. \tag{23a, b}$$

We are therefore able to describe all $2N$ values of λ in terms of the N values of Λ by means of equation (22).

If we define the vectors

$$(R_1^{\pm})_i = -\frac{1}{N_\Lambda^{\pm}} \frac{1}{X_k(\Lambda) \mp Y_k(\Lambda)} \frac{1}{\varepsilon_1(\boldsymbol{k}_i) - \Lambda}, \tag{24a}$$

$$(R_2^{\pm})_i = \frac{1}{N_\Lambda^{\pm}} \frac{1}{\varepsilon_1(\boldsymbol{k}_i) - \Lambda}, \tag{24b}$$

where

$$(N_\Lambda^{\pm}) = \pm \left(\sum_k \frac{2Y_k(\Lambda)}{Y_k(\Lambda) \mp X_k(\Lambda)} \frac{1}{\{\varepsilon_1(\boldsymbol{k}) - \Lambda\}^2} \right)^{\frac{1}{2}}, \tag{25}$$

then it is readily shown that the matrix of eigenvectors is

$$\hat{\mathbf{R}} = \begin{bmatrix} \hat{\mathbf{R}}_1^+ & \hat{\mathbf{0}} & \hat{\mathbf{R}}_1^- & \hat{\mathbf{0}} \\ \hat{\mathbf{0}} & \hat{\mathbf{R}}_1^+ & \hat{\mathbf{0}} & \hat{\mathbf{R}}_1^- \\ \hat{\mathbf{R}}_2^+ & \hat{\mathbf{0}} & \hat{\mathbf{R}}_2^- & \hat{\mathbf{0}} \\ \hat{\mathbf{0}} & \hat{\mathbf{R}}_2^+ & \hat{\mathbf{0}} & \hat{\mathbf{R}}_2^- \end{bmatrix}, \tag{26}$$

where $\hat{\mathbf{R}}_1^{\pm}$ and $\hat{\mathbf{R}}_2^{\pm}$ are matrices with vectors $\boldsymbol{R}_1^{\pm}$ and $\boldsymbol{R}_2^{\pm}$ as columns respectively.

The diagonal form of the crystal Hamiltonian is therefore

$$\mathscr{H} = \sum_\Lambda \left(\lambda^{(-)}(\Lambda)[\Phi_\Lambda^+ \Phi_\Lambda + \chi_\Lambda^+ \chi_\Lambda] + \lambda^{(+)}(\Lambda)[\Psi_\Lambda^+ \Psi_\Lambda + \Omega_\Lambda^+ \Omega_\Lambda] \right), \tag{27}$$

where the $\lambda^{(\pm)}$ correspond to the two sets of values of λ shown explicitly in equation (22), and

$$(\Phi_\Lambda, \chi_\Lambda) = \frac{1}{N_\Lambda^+} \sum_k \frac{(\alpha_k, \beta_k)}{[Y_k(\Lambda) - X_k(\Lambda)][\varepsilon_1(\boldsymbol{k}) - \Lambda]} + \frac{1}{N_\Lambda^+} \sum_k \frac{(A_k, B_k)}{\varepsilon_1(\boldsymbol{k}) - \Lambda}, \tag{28}$$

$$(\Psi_\Lambda, \Omega_\Lambda) = -\frac{1}{N_\Lambda^-} \sum_k \frac{(\alpha_k, \beta_k)}{[Y_k(\Lambda) + X_k(\Lambda)][\varepsilon_1(\boldsymbol{k}) - \Lambda]} + \frac{1}{N_\Lambda^-} \sum_k \frac{(A_k, B_k)}{\varepsilon_1(\boldsymbol{k}) - \Lambda}. \tag{29}$$

It can be shown that all these operators satisfy boson commutation rules and commute with each other.

The perturbation Hamiltonian (equation 15), when written in terms of the operators Φ, χ, Ψ and Ω becomes

$$\begin{aligned}\mathscr{H}_{\mathrm{P}} = -l\sum_{k}\sum_{\Lambda,\Lambda'}\big[&F_k^{++}(\Lambda,\Lambda')\left(\Phi_\Lambda^+\Phi_{\Lambda'}^+ + \Phi_\Lambda\Phi_{\Lambda'} + \chi_\Lambda^+\chi_{\Lambda'}^+ + \chi_\Lambda\chi_{\Lambda'}\right)\\ &+\left\{F_k^{+-}(\Lambda,\Lambda') + F_k^{-+}(\Lambda,\Lambda')\right\}\left(\Phi_\Lambda^+\Psi_{\Lambda'}^+ + \Phi_\Lambda\Psi_{\Lambda'} + \chi_\Lambda^+\Omega_{\Lambda'}^+ + \chi_\Lambda\Omega_{\Lambda'}\right)\\ &+F_k^{--}(\Lambda,\Lambda')\left(\Psi_\Lambda^+\Psi_{\Lambda'}^+ + \Psi_\Lambda\Psi_{\Lambda'} + \Omega_\Lambda^+\Omega_{\Lambda'}^+ + \Omega_\Lambda\Omega_{\Lambda'}\right)\big],\end{aligned} \tag{30}$$

where

$$F_k^{\pm\pm}(\Lambda,\Lambda') = \left[\frac{1}{N_\Lambda^{\pm}}\frac{1}{X_k(\Lambda)\mp Y_k(\Lambda)}\right]\left[\frac{1}{N_{\Lambda'}^{\pm}}\right]\frac{1}{\varepsilon_1(\boldsymbol{k})-\Lambda}\,\frac{1}{\varepsilon_1(\boldsymbol{k})-\Lambda'}. \tag{31}$$

In equation (31) the first and second $\pm$ superscripts to F refer to the first and second square brackets on the right-hand side of the equation respectively.

It is shown in the Appendix that $\mathscr{H}_{\mathrm{P}}$ (equation 30) may be simplified to the form:

$$\begin{aligned}\mathscr{H}_{\mathrm{P}} = -l\sum_{\Lambda}\big[&F_k^{++}(\Lambda,\Lambda)\left(\Phi_\Lambda^+\Phi_\Lambda^+ + \Phi_\Lambda\Phi_\Lambda + \chi_\Lambda^+\chi_\Lambda^+ + \chi_\Lambda\chi_\Lambda\right)\\ &+\left\{F_k^{+-}(\Lambda,\Lambda) + F_k^{-+}(\Lambda,\Lambda)\right\}\left(\Phi_\Lambda^+\Psi_\Lambda^+ + \Phi_\Lambda\Psi_\Lambda + \chi_\Lambda^+\Omega_\Lambda^+ + \chi_\Lambda\Omega_\Lambda\right)\\ &+F_k^{--}(\Lambda,\Lambda)\left(\Psi_\Lambda^+\Psi_\Lambda^+ + \Psi_\Lambda\Psi_\Lambda + \Omega_\Lambda^+\Omega_\Lambda^+ + \Omega_\Lambda\Omega_\Lambda\right)\big],\end{aligned} \tag{32}$$

with F_k^{++}, $F_k^{+-}+F_k^{-+}$ and F_k^{--} given by equations (A2), (A8) and (A6) respectively. The optical absorption of the system is now obtained from the nonzero Green's functions of the operator pairs shown in equation (32) (Richardson 1976*a*). The relevant Green's functions are

$$\langle\langle\Phi_\Lambda\Phi_\Lambda, \Phi_{\Lambda'}^+\Phi_{\Lambda'}^+\rangle\rangle = \frac{\delta(\Lambda,\Lambda')}{\hbar\omega - 2\lambda^{(-)}(\Lambda)} = \langle\langle\chi_\Lambda\chi_\Lambda, \chi_{\Lambda'}^+\chi_{\Lambda'}^+\rangle\rangle, \tag{33}$$

$$\langle\langle\Psi_\Lambda\Psi_\Lambda, \Psi_{\Lambda'}^+\Psi_{\Lambda'}^+\rangle\rangle = \frac{\delta(\Lambda,\Lambda')}{\hbar\omega - 2\lambda^{(+)}(\Lambda)} = \langle\langle\Omega_\Lambda\Omega_\Lambda, \Omega_{\Lambda'}^+\Omega_{\Lambda'}^+\rangle\rangle, \tag{34}$$

$$\langle\langle\Phi_\Lambda\Psi_\Lambda, \Phi_{\Lambda'}^+\Psi_{\Lambda'}^+\rangle\rangle = \frac{\delta(\Lambda,\Lambda')}{\hbar\omega - \{\lambda^{(+)}(\Lambda)+\lambda^{(-)}(\Lambda)\}} = \langle\langle\chi_\Lambda\Omega_\Lambda, \chi_{\Lambda'}^+\Omega_{\Lambda'}^+\rangle\rangle, \tag{35}$$

where we use the notation of equation (27).

The optical absorption of the system is obtained from the imaginary parts of equations (33)–(35). In particular, the magnon sideband lineshape is given from equations (32), (35) and (A8) as

$$\begin{aligned}\alpha(\omega) \approx\ &-\omega\sum_{\Lambda}\left[\left\{\sum_k X_k(\Lambda)H_k^2(\Lambda)\right\}\Big/\left\{\sum_k\left(\frac{Y_k}{Y_k-X_k}\right)_\Lambda H_k^2(\Lambda)\right\}^{\frac{1}{2}}\left\{\sum_k\left(\frac{Y_k}{Y_k+X_k}\right)_\Lambda H_k^2(\Lambda)\right\}^{\frac{1}{2}}\right]^2\\ &\times\delta\left(\hbar\omega - \{\lambda^+(\Lambda)+\lambda^-(\Lambda)\}\right),\end{aligned} \tag{36}$$

where we have defined

$$H_k(\Lambda) = \{\varepsilon_1(\boldsymbol{k})-\Lambda\}^{-1} \tag{37}$$

for convenience. The other two Green's functions (equations 33 and 34) give the two-magnon and two-exciton absorptions.

In principle, at least, the sums in equation (36) may be done, and the result will be that the magnon sideband lineshape is a modified impure crystal density of states. Because of the complicated evaluation required, however, it is thought to be adequate to give an example of the case when ε_2 and g are independent of $\boldsymbol{k}$, as this will point out the essential features of the sideband and its changes when an impurity is present. For this situation, equation (36) may be simplified to

$$\begin{aligned}\alpha(\omega) &\approx -\omega \sum \{X(\Lambda)/Y(\Lambda)\}^2 \delta(\hbar\omega - \varepsilon_2 - \Lambda) \\ &\approx -4\pi\omega \int \{X(\varepsilon)/Y(\varepsilon)\}^2 \delta(\hbar\omega - \varepsilon_2 - \varepsilon)\, \mathfrak{g}(\varepsilon)\, \mathrm{d}\varepsilon \\ &\approx -4\pi\omega \{X(\hbar\omega - \varepsilon_2)/Y(\hbar\omega - \varepsilon_2)\}^2\, \mathfrak{g}(\hbar\omega - \varepsilon_2), \end{aligned} \tag{38}$$

where Λ is now the eigenvalue of the magnon part of the Hamiltonian (as pointed out above) and $X(\Lambda)$ and $Y(\Lambda)$ are independent of wavenumber.

The function $\mathfrak{g}(\varepsilon)$ in equation (38) is the impure crystal magnon density of states, given by

$$\mathfrak{g}(\varepsilon) = \mathfrak{g}_0(\varepsilon) - \pi^{-1} \operatorname{Im}\left(\mathrm{d}\mathscr{D}(\varepsilon)/\mathrm{d}\varepsilon\right), \tag{39}$$

where $\mathfrak{g}_0(\varepsilon)$ is the pure crystal magnon density of states, and the second term represents the change of density of states due to the impurity. From equations (20) and (21), we now have

$$\mathscr{D}(\varepsilon) = 1 + \gamma \sum_{\boldsymbol{k}} \{\varepsilon_1(\boldsymbol{k}) - \varepsilon\}^{-1}. \tag{40}$$

Also, equation (23a) becomes

$$X(\Lambda) = (\varepsilon_2 - \Lambda)/2g,$$

so that we have

$$\left(\frac{X(\hbar\omega - \varepsilon_2)}{Y(\hbar\omega - \varepsilon_2)}\right)^2 = \frac{(2\varepsilon_2 - \hbar\omega)^2}{(2\varepsilon_2 - \hbar\omega)^2 + 4g^2}. \tag{41}$$

Now, as the sideband is located just on the high-energy side of ε_2, and since $\varepsilon_2 \gg g$, it follows that the ratio in equation (41) is in general very close to unity. Thus the magnon sideband lineshape is very accurately represented by the magnon density of states (equation 39).

4. Magnon Sideband in a Pure Perovskite Crystal

Many antiferromagnetic insulators have been found to exhibit magnon sideband behaviour. A good review of the observations of such crystals is given by Sell (1968) and also by Eremenko and Belyaeva (1969), and studies continue up to the present. The two most popular crystals for these studies are MnF_2 and $RbMnF_3$, the latter of which is considered here.

The crystal $RbMnF_3$ has a perovskite structure as shown in Fig. 1, with each magnetic ion at the corners of a simple cubic lattice. The lattice parameter is $a = 4{\cdot}26$ Å (Stokowski *et al.* 1971), the crystal being very highly isotropic, with a

negligible anisotropy field (Elliott *et al.* 1968). The magnetic properties of the Mn^{2+} ion are well summarized by Fujiwara *et al.* (1972) and Richards and Brya (1974). Fujiwara *et al.* also discussed the temperature dependence of magnon sidebands. The Néel temperature for this crystal is 83 K.

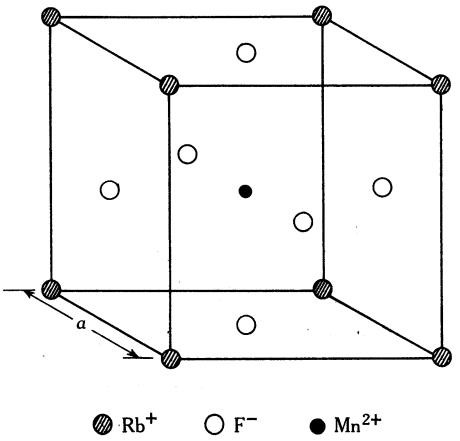

Fig. 1. Unit cell of the perovskite $RbMnF_3$. The Rb^+ ions appear at the cube vertices, Mn^{2+} ions at the body centre of the cube, and F^- ions at the centre of the cube faces. The magnetic Mn^{2+} ions form a simple cubic structure with lattice parameter α.

Richards and Brya (1974) gave the value of the nearest neighbour exchange integral in $RbMnF_3$ as $2J = 4{\cdot}7\ \mathrm{cm}^{-1}$ with an uncertainty of $\pm 0{\cdot}25\ \mathrm{cm}^{-1}$ at 300 K, a value which agrees well with the results of many other authors. As has been pointed out (e.g. by Srivastava and Stevenson 1972) the next nearest neighbour exchange integral is $0 \pm 0{\cdot}14\ \mathrm{cm}^{-1}$ (for $2J_2$) and hence is negligible. The anisotropy field is also negligible. Using the value of $2J$ given, we may obtain the maximum magnon energy from the expression for the perovskite magnon dispersion of

$$\varepsilon(\boldsymbol{k}) = \varepsilon_0[1 - \tfrac{1}{9}\{\cos(k_x\alpha) + \cos(k_y\alpha) + \cos(k_z\alpha)\}^2]^{\frac{1}{2}},$$

where

$$\varepsilon_0 = 12JS. \tag{42}$$

For a ground state spin of 5/2 this gives a value for ε_0 of $71\ \mathrm{cm}^{-1}$, with the limits on $2J$ giving a range from 67 to $74\ \mathrm{cm}^{-1}$. Hence one would expect the magnon sideband cutoff to have a value near this, though Srivastava and Stevenson (1972) pointed out that the uncertainty in the next nearest neighbour exchange integral $2J_2$ of $\pm 0{\cdot}14\ \mathrm{cm}^{-1}$ could allow ε_0 to lie within the range 55 to $89\ \mathrm{cm}^{-1}$, which would account for the variation in the value of the cutoff observed for various transitions in $RbMnF_3$ with a ground state spin of 5/2.

From equation (38) the predicted magnon sideband shape for a transition in $RbMnF_3$ will be given very closely by the pure crystal magnon density of states. The latter is shown in Fig. 2 for the range normalized to the interval [0, 1]. Note the cusp point at $\sqrt{(8/9)}$ due to the symmetry point X of the first Brillouin zone, and the divergence at the high energy end of the band due to the symmetry points L and W in the Brillouin zone (Eremenko *et al.* 1974).

From Fig. 2 we would expect the magnon sideband to have its peak at the cutoff point, and to have a width which is approximately $\{1-\sqrt{(8/9)}\}$th of the distance between the parent exciton frequency and the cutoff frequency. This sort of

behaviour has been measured (e.g. Stevenson 1966) for the $^6A_{1g}(^6S) \rightarrow {}^4E_g(^4G)$ transition, which has also been studied in some detail by Srivastava and Stevenson (1972) and Eremenko *et al.* (1974).

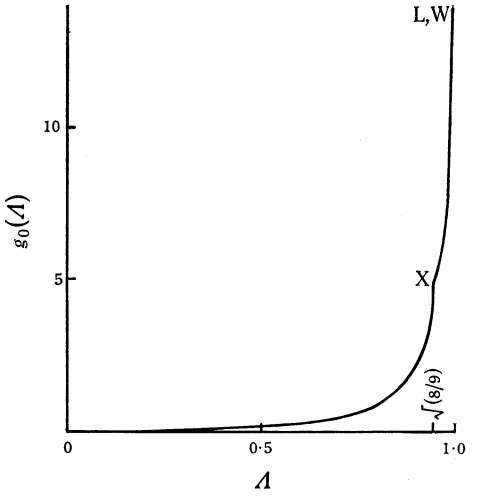

Fig. 2. Plot of the pure crystal magnon density of states as a function of the frequency Λ, normalized to the range [0, 1], for an antiferromagnetic perovskite crystal. The calculated lineshape is a very good approximation to this curve.

In reality we must include next nearest neighbours in the magnon dispersion equation (42) and this will remove the logarithmic singularity at the upper edge of the band, making the result more physically reasonable. As pointed out in the Conclusions (below) the effect of a $\boldsymbol{k}$-dependent exciton–magnon interaction strength $g(\boldsymbol{k})$ which is large near the edge of the Brillouin zone will also contribute to the removal of the singularity. Also, if the symmetry of the two-ion site involved in the exciton–magnon interaction is more rigorously accounted for then the cusp point at $\Lambda = \sqrt{(8/9)}$ due to the point X in the Brillouin zone will be removed (Parkinson and Loudon 1968).

5. Effect of Impurity on a Sideband in Perovskite

The analysis of the effects of an impurity on a magnon sideband in the present case is very similar to that for the ferromagnet (Richardson 1976*a*). In particular, it is necessary for the following condition to hold for there to be local modes outside the band:

$$1 + \gamma R(\Lambda) = 0, \tag{43}$$

for Λ lying outside the band. In equation (43) $R(\Lambda)$ is the Hilbert transform of the density of states $g(\Lambda)$ which is nonzero only for the in-band region of the spectrum. A resonance will appear within the band if (Richardson 1976*a*)

$$1 + \gamma R(\Lambda) = 0 \qquad (\Lambda = \Lambda_0 \text{ inside the band}), \tag{44a}$$

$$\Gamma = [2\pi g_0(\Lambda)/R'(\Lambda)]_{\Lambda=\Lambda_0} < 0, \tag{44b}$$

$$|\Gamma| \ll 1. \tag{44c}$$

We now consider a particular example: Johnson *et al.* (1966) have reported on the

effects of Ni^{2+} impurities on the emission spectra of MnF_2, $KMnF_3$ and $RbMnF_3$. Unfortunately the spectrum taken in emission is complicated because of the possibility of different coupling of the excitons and magnons with each other and with the radiation field. Therefore it is likely that the model Hamiltonians we have chosen specifically to study absorption effects may not describe the situation very well. This is confirmed by the occurrence of sidebands lower in energy than the parent excitons, and for energies of separation much larger than $\varepsilon_0 \approx 70\ \mathrm{cm}^{-1}$ in the case of $RbMnF_3$, as expected. The sidebands at lower energy than the parent are probably highly temperature-dependent 'hot bands' (Sell 1968). We therefore conclude that we are unable to describe the phenomena observed by Johnson *et al.* with the present model calculations. It should be noted, however, that their value for the impurity–host exchange integral J', given in terms of the pure crystal value J, was

$$J'/J = 3{\cdot}5 \tag{45}$$

for Ni^{2+} in a host of Mn^{2+} ions. Since from equation (9), γ is approximated by

$$\gamma \approx 2JSz\varepsilon = 2JSz(J'/J - 1), \tag{46}$$

we see that γ is positive, with a value of $2{\cdot}5\,\varepsilon_0$ for ε_0, and that we have the magnon dispersion energy given by equation (42) for the perovskite structure.

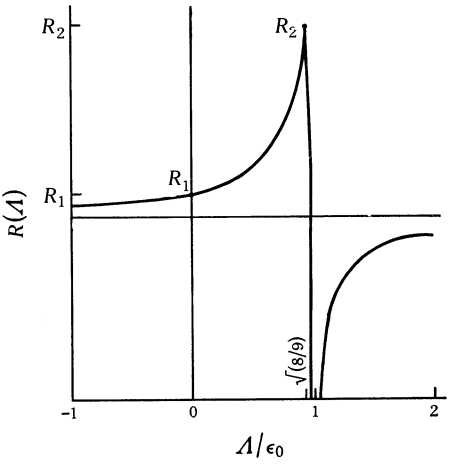

Fig. 3. Plot of the real part $R(\Lambda)$ of the lattice Green's function for a perovskite structure crystal such as $RbMnF_3$. The energy has been normalized so that the pure absorption band lies between 0 and 1.

In Fig. 3 we present the curve of $R(\Lambda)$ for the perovskite structure which has the magnetic ions arranged antiferromagnetically on a simple cubic lattice. This curve is the Hilbert transform of the pure crystal density of states $g_0(\Lambda)$ shown in Fig. 2. Following the discussion of Richardson (1976*a*), as summarized above, a local mode will occur whenever γ is positive, or for γ negative and sufficiently large that

$$0 < -1/\gamma < R_1\,. \tag{47}$$

For γ positive the local mode is on the high energy side of the band, while for condition (47) it lies on the low energy side.

There is also the possibility of resonant modes appearing for the range

$$R_1 < -1/\gamma < R_2\,, \tag{48}$$

since in this range equation (44a) is satisfied. For resonance modes to occur the conditions (44b) and (44c) must be met for γ satisfying (48). The second of these conditions will apply if Λ is greater than the cusp point of Fig. 3 at $\sqrt{(8/9)}$. We must thus examine the criterion (44c) for

$$1{\cdot}0 > \lambda > \sqrt{(8/9)} \tag{49}$$

and γ satisfying (48).

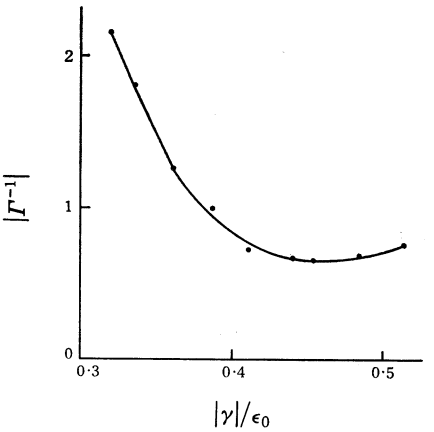

Fig. 4. Plot of numerical calculations of possible resonant mode lifetimes $|\Gamma^{-1}|$ as a function of $|\gamma|/\varepsilon_0$ for the perovskite crystal and for γ and λ satisfying the conditions (48) and (49) respectively. The range of γ/ε_0 satisfying the condition (48) is $-0{\cdot}32 \leqslant \gamma/\varepsilon_0 \leqslant -2{\cdot}7$. The range shown is where the lifetime is largest. Data for $\gamma \lesssim -0{\cdot}4$ are highly inaccurate.

The lifetimes $|\Gamma^{-1}|$ for possible resonance modes of the perovskite structure are plotted in Fig. 4. The largest lifetime is found to occur for $-1/\gamma$ very close to R_2, but the lifetime of about $2{\cdot}1$ is not sufficiently larger than unity for the resonance to be observable, though the lifetime for this structure is longer than that for the ferromagnetic f.c.c. structure. Another complication in this case is the greater proximity of points of possible resonance to the divergence of the density of states at the band edge (Fig. 2) which will make any other close maximum in the density of states difficult to resolve.

We may therefore summarize the expected effects of a substitutional spin impurity on a perovskite structure crystal like $RbMnF_3$ as follows: Local modes will occur for γ positive, and for negative values of γ sufficiently large to satisfy the condition (47).* When local modes exist there will be only small, and probably unobservable, changes to the in-band region of the spectrum. For the Ni^{2+} impurity studied by Johnson *et al.* (1966) there will be a local mode at an energy of $\sim 0{\cdot}71$ times the bandwidth higher than the top of the band in the absorption spectrum.

In the region of the spectrum satisfied by the condition (49) and for γ satisfying the condition (48), the possibility of the appearance of resonance modes was explored and it was found that, although the lifetime of states in this region is longer than that for the ferromagnetic f.c.c. structure studied by Richardson (1976*a*), the lifetimes are not sufficiently long for a resonance to become observable. Hence for all values of γ such that

$$-1/\gamma > R_1, \tag{50}$$

* The condition that γ is negative may be fulfilled if the impurity couples ferromagnetically to the host crystal, though in this case interband scattering of magnons may not be negligible and it may not be reasonable to ignore the effect of the off-diagonal submatrices $\hat{\mathbf{M}}_2$ and $\hat{\mathbf{M}}_3$ of equation (3).

it is expected that the impurity will not have any observable effect on the magnon sideband lineshape.

Parkinson (1969*a*, 1969*b*) also studied impurity effects on the magnon sidebands of $RbMnF_3$ and concluded that local modes (for s_0 symmetry modes localized on the impurity) will occur above the band for $\varepsilon > 0$, that is, in our case for $\gamma > 0$ (equation 46) apart from any effect of anisotropy fields (small in $RbMnF_3$). He did not mention any condition for the appearance of local modes below the band, however. Parkinson (1969*b*) discussed resonance modes within the band but did not give any strong arguments for their existence, or otherwise. It would thus appear that the present simple model is capable of explaining many of the impurity phenomena discussed by Parkinson (1969*a*, 1969*b*) with his more sophisticated model, but also permits a discussion of the existence of resonant modes within the band in a semi-qualitative manner.

6. Conclusions

This paper has presented a model calculation of a magnon sideband in an antiferromagnetic crystal, and discussed the effect that a substitutional spin impurity will have on it. The calculation is based on an earlier model of a ferromagnetic crystal (Richardson 1974, 1976*a*). The drastic approximations which are implicit in the forms of the Hamiltonians used are necessary for one to be able to obtain a solution to the problem when both exciton–magnon interaction and magnon–impurity effects are considered. The form for the exciton–magnon interaction may be justified from more rigorous four-operator forms when one realizes that Green's functions calculated from the latter must be approximated usually by extraction of an equal-time average from the Green's function, reducing it to a form with two operators. It can be shown that the same resultant form can be obtained from a phenomenological two-operator form (Richardson 1976*b*), though the analysis is not given here. It has been shown by Richardson (1976*b*) that a more exact form for the impurity Hamiltonian may be treated rigorously within the framework, but a simpler model was used here in order to discuss the physical effects of impurities on magnon sidebands without mathematical complexity.

Apart from the twofold degeneracy introduced by the two sublattices, comparison of the expression (38) for the sideband derived here (with ε_2 and g both $\boldsymbol{k}$-independent) with that for the ferromagnet (Richardson 1976*a*) shows that the form of the expressions is identical (apart from the factor of two) though, of course, the densities of states will differ in the two cases.

Apart from the factor shown in equation (41), which is very nearly constant throughout the bandwidth of the sideband for a given value of the exciton–magnon interaction strength g, the pure crystal sideband lineshape is given by the pure magnon density of states (illustrated for the perovskite crystal in Fig. 2). A comparison of this shape with the experimental data of Stevenson (1966) on $RbMnF_3$ shows qualitative similarity. The shape is also very similar to calculated sideband shapes when there is no exciton–magnon interaction, because of the weak dependence of the lineshape on g when g is taken as constant throughout the Brillouin zone in the present case (e.g. Eremenko *et al.* 1967; Parkinson and Loudon 1968).

In Part I we speculated that inclusion of a $\boldsymbol{k}$-dependence of the exciton–magnon interaction strength g could have a significant effect on the sideband lineshape, as

found by Parkinson and Loudon (1968), provided $g(\boldsymbol{k})$ was large near the edge of the band. We have here been able to derive the exact antiferromagnetic expression for the magnon sideband lineshape with $\boldsymbol{k}$-dependent g. By inspection of the result (36), it is expected that the factors X_k and Y_k will make a significant contribution to the lineshape since, if $g(\boldsymbol{k})$ is large near the edge of the band, the assumption that $X_k = Y_k$ may no longer be valid. In fact Y_k may be larger than X_k, so that the lineshape will be diminished near the edge of the band and have a maximum within the band, as found by Parkinson and Loudon (1968).

The present calculation also makes it possible to take into account the dispersion of the excitons within the Brillouin zone. Although this is usually much smaller than the magnon dispersion, there is no reason to expect that the effect is not observable in some cases. Meltzer *et al.* (1969), for example, found that they could obtain a more satisfactory comparison between the observed and theoretical lineshape for MnF_2 if they assumed some exciton dispersion, although they neglected the effect of an exciton–magnon interaction in their calculation.

Acknowledgments

The author would like to thank Dr K. Kumar and Dr J. Mahanty for their help and encouragement during the course of this work. The work was supported by a Commonwealth Postgraduate Research Award, supplemented by the Australian National University.

References

Bhandari, R., and Falicov, L. M. (1972). *J. Phys.* C **5**, 1445–60.
Callaway, J. (1974). 'Quantum Theory of the Solid State', Part B (Academic: New York).
Dietz, R. E., Meixner, A. E., and Guggenheim, H. J. (1970). *J. Lumin.* **1**, 279–98.
Elliott, R. J., Thorpe, M. F., Imbusch, G. F., Loudon, R., and Parkinson, J. B. (1968). *Phys. Rev. Lett.* **21**, 147–50.
Eremenko, V. V., and Belyaeva, A. I. (1969). *Sov. Phys. Usp.* **12**, 320–43.
Eremenko, V. V., Novikov, V. P., and Petrov, E. G. (1974). *J. Low Temp. Phys.* **16**, 431–54.
Eremenko, V. V., Popkov, Yu. A., Novikov, V. P., and Belyaeva, A. I. (1967). *Sov. Phys. JETP* **25**, 297–302.
Freeman, S., and Hopfield, J. J. (1968). *Phys. Rev. Lett.* **21**, 910–13.
Fujiwara, T., Gebhardt, W., Petanides, K., and Tanabe, Y. (1972). *J. Phys. Soc. Jpn* **33**, 39–48.
Gaididei, Yu. B., and Loktev, V. M. (1974). *Phys. Status. Solidi* B **62**, K29–32.
Gondiara, K., and Tanabe, Y. (1966). *J. Phys. Soc. Jpn* **21**, 1527–48.
Halley, J. W., and Silvera, I. (1965). *Phys. Rev. Lett.* **15**, 654–6.
Johnson, L. F., Dietz, R. E., and Guggenheim, H. J. (1966). *Phys. Rev. Lett.* **17**, 13–15.
Knox, R. S. (1963). *Solid State Phys. Suppl.* No. 5.
Loudon, R. (1968). *Adv. Phys.* **17**, 243–80.
McClure, D. S. (1968). *In* 'Excitons, Magnons and Phonons' (Ed. Zahlan), pp. 135–52.
Meltzer, R. S., Lowe, M., and McClure, D. S. (1969). *Phys. Rev.* **180**, 561–78.
Misetich, A., Dietz, R. E., and Guggenheim, H. J. (1968). *In* 'Localised Excitations in Solids' (Ed. R. F. Wallis), pp. 379–85 (Plenum: New York).
Moriya, T. (1966). *J. Phys. Soc. Jpn* **21**, 926–32.
Moriya, T. (1968). *J. Appl. Phys.* **39**, 1042–9.
Moriya, T., and Inoue, M. (1968). *J. Phys. Soc. Jpn* **24**, 1251–64.
Parkinson, J. B. (1969*a*). *J. Appl. Phys.* **40**, 993–4.
Parkinson, J. B. (1969*b*). *J. Phys.* C **2**, 2003–11.
Parkinson, J. B., and Loudon, R. (1968). *J. Phys.* C **1**, 1568–83.
Petrov, E. G. (1971). *Phys. Status Solidi* B **48**, 367–79.

Petrov, E. G., and Gaididei, Yu. B. (1971). *Phys. Status Solidi* B **46**, 103–16.
Richards, P. M., and Brya, W. J. (1974). *Phys. Rev.* B **9**, 3044–52.
Richardson, D. D. (1974). *Aust. J. Phys.* **27**, 457–70.
Richardson, D. D. (1976*a*). *Aust. J. Phys.* **29**, 273–88.
Richardson, D. D. (1976*b*). Ph.D. Thesis, Australian National University.
Sell, D. D. (1968). *J. Appl. Phys.* **39**, 1030–5.
Sell, D. D., Greene, R. L., and White, R. M. (1967). *Phys. Rev.* **158**, 489–510.
Srivastava, V. C., and Stevenson, R. (1972). *Solid State Commun.* **11**, 41–6.
Stevenson, R. (1966). *Phys. Rev.* **152**, 531–5.
Stokowski, S. E., Sell, D. D., and Guggenheim, H. J. (1971). *Phys. Rev.* B **4**, 3141–52.
Tanabe, Y., and Gondiara, K.-I. (1967). *J. Phys. Soc. Jpn* **22**, 573–81.
Tanabe, Y., Gondiara, K.-I., and Murata, H. (1968). *J. Phys. Soc. Jpn* **25**, 1562–75.
Tanabe, Y., Moriya, T., and Sugano, S. (1965). *Phys. Rev. Lett.* **15**, 1023–5.

Appendix

The simplification of equation (30) is achieved as follows. We begin by considering the first term of this equation. We wish to evaluate

$$\sum_{\boldsymbol{k}} F_{\boldsymbol{k}}^{++}(\Lambda,\Lambda') = \sum_{\boldsymbol{k}} \frac{1}{N_{\Lambda}^{+}} \frac{1}{X_{\boldsymbol{k}}(\Lambda)-Y_{\boldsymbol{k}}(\Lambda)} \frac{1}{N_{\Lambda'}^{+}} \frac{1}{\varepsilon_1(\boldsymbol{k})-\Lambda} \frac{1}{\varepsilon_1(\boldsymbol{k})-\Lambda'}, \tag{A1}$$

making use of equation (31). When $\Lambda = \Lambda'$ equation (A1) becomes

$$\sum_{\boldsymbol{k}} F_{\boldsymbol{k}}^{++}(\Lambda,\Lambda) = \sum_{\boldsymbol{k}} \left(\frac{1}{X_{\boldsymbol{k}}-Y_{\boldsymbol{k}}}\right)_{\Lambda} \left(\frac{1}{\varepsilon_1(\boldsymbol{k})-\Lambda}\right)^2 \Big/ \sum_{\boldsymbol{k}} \left(\frac{2Y_{\boldsymbol{k}}}{Y_{\boldsymbol{k}}-X_{\boldsymbol{k}}}\right)_{\Lambda} \left(\frac{1}{\varepsilon_1(\boldsymbol{k})-\Lambda}\right)^2, \tag{A2}$$

using equation (25) for N_{Λ}^{+}.

When $\Lambda \neq \Lambda'$ we have

$$\begin{aligned}\sum_{\boldsymbol{k}} F_{\boldsymbol{k}}^{++}(\Lambda,\Lambda') &= \frac{1}{N_{\Lambda}^{+} N_{\Lambda'}^{+}} \sum_{\boldsymbol{k}} \frac{1}{X_{\boldsymbol{k}}(\Lambda)-Y_{\boldsymbol{k}}(\Lambda)} \frac{1}{\Lambda-\Lambda'} \left(\frac{1}{\varepsilon_1(\boldsymbol{k})-\Lambda} - \frac{1}{\varepsilon_1(\boldsymbol{k})-\Lambda'}\right) \\ &= \frac{1}{N_{\Lambda}^{+} N_{\Lambda'}^{+}} \sum_{\boldsymbol{k}} \frac{1}{X_{\boldsymbol{k}}(\Lambda')-Y_{\boldsymbol{k}}(\Lambda')} \frac{1}{\Lambda-\Lambda'} \left(\frac{1}{\varepsilon_1(\boldsymbol{k})-\Lambda} - \frac{1}{\varepsilon_1(\boldsymbol{k})-\Lambda'}\right) \\ &= 0, \end{aligned} \tag{A3}$$

since the two sums are identical. This is made clear, for example, when X and Y are independent of $\boldsymbol{k}$, by making use of the secular equation. Therefore we have the result

$$\sum_{\boldsymbol{k}} F_{\boldsymbol{k}}^{++}(\Lambda,\Lambda') = \delta(\Lambda,\Lambda') \sum_{\boldsymbol{k}} F_{\boldsymbol{k}}^{++}(\Lambda,\Lambda). \tag{A4}$$

The third term of equation (30) may be simplified along the same lines as the first to give

$$\sum_{\boldsymbol{k}} F_{\boldsymbol{k}}^{--}(\Lambda,\Lambda') = \delta(\Lambda,\Lambda') \sum_{\boldsymbol{k}} F_{\boldsymbol{k}}^{--}(\Lambda,\Lambda), \tag{A5}$$

where

$$\sum_{\boldsymbol{k}} F_{\boldsymbol{k}}^{--}(\Lambda,\Lambda) = \sum_{\boldsymbol{k}} \left(\frac{1}{X_{\boldsymbol{k}}+Y_{\boldsymbol{k}}}\right)_{\Lambda} \left(\frac{1}{\varepsilon_1(\boldsymbol{k})-\Lambda}\right)^2 \Big/ \sum_{\boldsymbol{k}} \left(\frac{2Y_{\boldsymbol{k}}}{X_{\boldsymbol{k}}-Y_{\boldsymbol{k}}}\right)_{\Lambda} \left(\frac{1}{\varepsilon_1(\boldsymbol{k})-\Lambda}\right)^2. \tag{A6}$$

The second term of equation (30) gives

$$\sum_k \{F_k^{+-}(\Lambda,\Lambda') + F_k^{-+}(\Lambda,\Lambda')\}$$
$$= \sum_k \left(\frac{1}{N_\Lambda^+ N_{\Lambda'}^-} \frac{1}{X_k(\Lambda) - Y_k(\Lambda)} + \frac{1}{N_\Lambda^- N_{\Lambda'}^+} \frac{1}{X_k(\Lambda) + Y_k(\Lambda)}\right)$$
$$\times \left(\frac{1}{\varepsilon_1(\boldsymbol{k}) - \Lambda} \frac{1}{\varepsilon_1(\boldsymbol{k}) - \Lambda'}\right). \tag{A7}$$

When $\Lambda = \Lambda'$ we have

$$\sum_k \{F_k^{+-}(\Lambda,\Lambda) + F_k^{-+}(\Lambda,\Lambda)\} = \sum_k \frac{1}{N_\Lambda^+ N_\Lambda^-} \frac{2X_k(\Lambda)}{X_k^2(\Lambda) - Y_k^2(\Lambda)} \left(\frac{1}{\varepsilon_1(\boldsymbol{k}) - \Lambda}\right)^2$$
$$= -\frac{\sum_k X_k(\Lambda) \left(\frac{1}{\varepsilon_1(\boldsymbol{k}) - \Lambda}\right)^2}{\left[\sum_k \left(\frac{Y_k}{Y_k - X_k}\right)_\Lambda \left(\frac{1}{\varepsilon_1(\boldsymbol{k}) - \Lambda}\right)^2\right]^{\frac{1}{2}} \left[\sum_k \left(\frac{Y_k}{Y_k + X_k}\right)_\Lambda \left(\frac{1}{\varepsilon_1(\boldsymbol{k}) - \Lambda}\right)^2\right]^{\frac{1}{2}}}. \tag{A8}$$

When $\Lambda \neq \Lambda'$ we may use the arguments that lead to the vanishing of the first term of equation (30) to show that the sum (A8) is zero. Therefore we have the result

$$\sum_k \{F_k^{+-}(\Lambda,\Lambda') + F_k^{-+}(\Lambda,\Lambda')\} = \delta(\Lambda,\Lambda') \sum_k \{F_k^{+-}(\Lambda,\Lambda) + F_k^{-+}(\Lambda,\Lambda)\}. \tag{A9}$$

For the particular example discussed in the text, where X and Y are independent of $\boldsymbol{k}$, the results (A4), (A5) and (A9) reduce to

$$\sum_k F_k^{++}(\Lambda,\Lambda') = \{-1/2Y(\Lambda)\}\,\delta(\Lambda,\Lambda'), \tag{A4a}$$

$$\sum_k F_k^{--}(\Lambda,\Lambda') = \{-1/2Y(\Lambda)\}\,\delta(\Lambda,\Lambda'), \tag{A5a}$$

$$\sum_k \{F_k^{+-}(\Lambda,\Lambda') + F_k^{-+}(\Lambda,\Lambda')\} = -\{X(\Lambda)/Y(\Lambda)\}\,\delta(\Lambda,\Lambda'). \tag{A9a}$$

The results (A4), (A5) and (A9) are readily used to write $\mathscr{H}_{\mathrm{P}}$ in the form shown in equation (32).

Manuscript received 28 January 1976